

## **First Results from the ISO-IRAS Faint Galaxy Survey'**

Deborah A. Levine<sup>2,3</sup>, Carol J. Lonsdale<sup>2</sup>, Robert L. Hurt<sup>2</sup>, Harding E. Smith<sup>4,2</sup>, George Helou<sup>2</sup>,  
Charles A. Beichman<sup>2</sup>, Catherine J. Cesarsky<sup>5</sup>, David El baz<sup>5</sup>, Ulrich Klaas<sup>3</sup>, Rene Laureijs<sup>3</sup>,  
Detrich Lemke<sup>6</sup>, Steven D. Lord<sup>2</sup>, Richard G. McMahon<sup>7</sup>, Mehrdad Moshir<sup>2</sup>, Gerry Neugebauer<sup>8</sup>,  
B. T. Soifer<sup>8</sup>, Dave Van Buren<sup>2</sup>, Ann E. Wehrle<sup>2</sup>, Ray D. Wolstencroft<sup>9</sup>

Received \_\_\_\_\_) accepted \_\_\_\_\_

---

ISO is an ESA project with instruments funded by ESA member states (especially the PI countries; France, Germany, the Netherlands and the United Kingdom) and with the participation of ISAS and NASA

<sup>2</sup>Infrared Processing & Analysis Center, Caltech/JPL, Pasadena, CA 91125

<sup>3</sup>ISO Science Operations Centre, Villafranca Apdo 50727, E-28080 Madrid, Spain

<sup>4</sup>Center for Astrophysics & Space Sciences, University of California, San Diego, CA 92093-0424

<sup>5</sup>Service d'Astrophysique, DSM, CEA-Saclay, F-91191 Gif-sur-Yvette Cedex, France

<sup>6</sup>Max-Planck-Institut für Astronomie, Königstuhl 17, D-69117 Heidelberg, Germany

<sup>7</sup>Institute for Astronomy, Madingley Road, Cambridge CB3 0HA, England

<sup>8</sup>California Institute of Technology, Pasadena CA 91125

<sup>9</sup>Royal Observatory, Blackford Hill, Edinburgh EH9 3HJ, Scotland

## ABSTRACT

We present the first results from the ISO-IRAS Faint Galaxy Survey (IIFGS), a program designed to obtain ISO observations of the most distant and luminous galaxies in the IRAS Faint Source Survey by filling short gaps in the ISO observing schedule with pairs of 12 $\mu$ m ISOCAM and 90 $\mu$ m ISOPHOT observations. As of October 1997, over 500 sources have been observed, with an ISOCAM detection rate over 80%, covering over 1.25 square degrees of sky to an 11.5 $\mu$ m point source completeness limit of approximately 1.0 mJy (corresponding to an  $\sim 10\sigma$  detection sensitivity). In this paper we present results for 9 sources detected early in the survey for which we have ground-based G and I band images and optical spectroscopy. The ground-based data confirms that the IIFGS strategy efficiently detects moderate-redshift ( $z = 0.11 - 0.38$  for this small sample) strong emission line galaxies with  $L_{60} \gtrsim 10^{11} L_{\odot}$ ; one of our sample has  $L_{60} > 10^{12} L_{\odot}$  ( $H_0 = 75 \text{ km s}^{-1} \text{ Mpc}^{-1}$ ,  $\Omega = 1$ ). The infrared-optical spectral energy distributions are comparable to those of nearby luminous infrared galaxies which span the range from pure starburst (eg Arp 220) to infrared QSO (Mrk 231). Two of the systems show signs of strong interaction, and four show AGN-like excitation; one of the AGN, F15390+6038, which shows a high excitation Sy2 spectrum, has an unusually warm far-to mid-infrared color and may be an obscured QSO. The IIFGS sample is one of the largest and deepest samples of infrared-luminous galaxies available, promising to be a rich sample for studying Luminous Infrared Galaxies up to  $z \sim 1$  and for understanding the evolution of infrared galaxies and the star-formation rate in the Universe.

*Subject headings:* galaxies: active — galaxies: starburst — infrared: galaxies

## 1. Introduction

IRAS discovered thousands of luminous infrared-bright galaxies (LIGs) which emit most (over 90% in some cases) of their luminosity in the far infrared. These infrared-luminous galaxies dominate the space density of objects with  $L > 10^{11} L_{\odot}$  (Soifer *et al.* 1987). Most of these objects are probably primarily powered by starbursts, but there is also evidence of AGN activity, especially at the higher luminosities (Sanders & Mirabel 1996). ‘There has been speculation that protogalaxies may appear as high-redshift LIGs, but the two very high redshift systems, F10214+4724 and ‘the cloverleaf’ both appear to be lensed AGN systems (Eisenhardt *et al.* 1996, Barvainis *et al.* 1995).

The IRAS Bright Galaxy Sample (BGS) (Soifer *et al.* 1987), complete to 5.24 Jy at  $60\mu\text{m}$ , provides an excellent sample of local infrared-luminous galaxies for studying the detailed emission mechanisms and starburst-AGN connections, but a determination of how these properties evolve with time, as well as searching for protogalaxy candidates requires a large sample well distributed in redshift. The IRAS Faint Source Survey (FSS) (Moshir *et al.* 1995) contains over 750,000 sources to a  $60\mu\text{m}$  flux density limit as faint as 100 mJy in some regions of sky, which is over 50 times fainter than the limit of the BGS. The vast majority of these faint sources have not been followed up in any way. The ISO mission presents an ideal opportunity to obtain infrared spectral information for a subset of these objects, as well as much better positional information from ISOCAM than available from the large IRAS  $60\mu\text{m}$  detectors.

The ISO-IRAS Faint Galaxy Survey (IIFGS) consists of 3776 of sources from the FSS selected to be fainter than 300 mJy at  $60\mu\text{m}$  with galaxy-like infrared colors, to have galactic latitude  $>30^{\circ}$  (to avoid contamination by Galactic sources), and to have a high value of the  $S_{60\mu\text{m}}/S_{\text{blue}}$  flux density ratio. The combination of faintness at  $60\mu\text{m}$  and high value of  $S_{60\mu\text{m}}/S_{\text{blue}}$  leads to a selection in favor of the most luminous and highest redshift candidates since there is a strong

---

‘Sources were selected from the entire FSS, not just the Faint Source Catalog (FSC) to reach the faintest possible IRAS limits. Source reliability was assured by insisting on a good optical match to each source and a robust  $60\mu\text{m}$  detection on coadded scan tracks using IPAC’s Scanpi processor.

correlation between  $L_{FIR}$  and  $L_{60\mu m}/L_{blue}$  for infrared-bright galaxies (Soifer *et al.* 1987). Blue magnitudes for each candidate source were obtained from the IPAC's OPTID service (Lonsdale *et al.* 1997); 60pm sources were selected if they have a blue counterpart fainter than about 17.5 msg. in the northern sky and 19 msg. in the southern sky (a lower magnitude limit was required in the northern sky to obtain a balance in the total number of sources available in each hemisphere). Great care was taken to eliminate contamination by cirrus sources from the sample. The details of the source selection for the IIFGS are given elsewhere (Lonsdale *et al.* 1998a). OPTID finding charts for 9 sources reported here are shown in Figure 1.

The IIFGS sample galaxies are scheduled for observation by 1S0 on a “Filler” basis; IIFGS sources are selected to fill gaps in the 1S0 observing schedule once higher priority targets have been scheduled. Thus the IIFGS serves to enhance the total observing efficiency of the mission. Of the 3776 candidate IIFGS sources in the 1S0 observation database, over 500 have been observed as of 1997 October and it is expected that over 600 will be observed before the end of the 1S0 mission, with a total solid angle coverage of nearly 1.5 square degrees on the sky.

The IIFGS sample will represent one of the best and largest deep samples of infrared-luminous galaxies until the advent of WIRE (Wide Field Infrared Explorer; Hacking *et al.* 1996) and SIRTF, even though it is based on selection from the fourteen year old IRAS survey. 1S0 cannot easily probe significantly deeper in redshift than the IRAS Faint Source Survey because the excellent sensitivity of ISOCAM is offset by the declining infrared spectral energy distribution from 60pm (the most sensitive IRAS band for galaxies) to the shorter mid-infrared wavelengths of ISOCAM.

## 2. Observations

We present data for 9 of the IIFGS galaxies obtained with the Infrared Space Observatory (1S0) (Kessler *et al.* 1996) using the camera ISOCAM (Cesarsky *et al.* 1996) at 12pm and the photometer ISOPHOT (Lemke *et al.* 1996) at 90pm. Optical spectra and G and I band images were obtained at Lick Observatory.

## 2.1. ISOCAM Observations

The ISOCAM data presented in this paper consist of short “micro scan” maps that have been optimized for maximum sensitivity, using the LW array, which is a 32x32 pixel gallium doped silicon array. The LW10 (“IRAS12 $\mu$ m”) filter, centered at a wavelength of 11.5  $\mu$ m was employed because of its large bandwidth of 7  $\mu$ m, and the plate scale of 6”/pixel maximizes the collecting area of each pixel. Each field was observed using a 2 x 2 microscan with 5 pixel (30”) offsets in the satellite coordinate system, producing a fully sampled field of view of  $\sim 2.7' \times 2.7'$ . An integration time of 2.1 sec was used for each frame. Each observation consisted of  $\sim 12$  stabilization frames (allowing the detector to respond to the sky background),  $\sim 6$  frames at each raster position, and  $\sim 2$  frames between rasters during slews, for a total on-source integration time of about 90 sees. ,

The ISOCAM data were reduced using custom software in development at IPAC. The Standard Processed Data (SPD) product of the On-Line Processing (01.1') versions 4.1 to 5.3 were employed for the reduction process. While a more detailed discussion of this technique will be forthcoming (Hurt *et al.* 1998) the basic steps are outlined here. Cosmic ray hits are first identified and flagged using the multi-resolution median deglitcher (MR1D\_DEGLITCH, a component of the CAM , Interactive Analysis package) which looks for glitches on short temporal scales and works well with unstabilized data. The next critical step is to correct for the “transient” response of the ISOCAM detectors. The time required for the detectors to stabilize to the zodiacal backgrounds in these fields is comparable to the length of our observations. In order to construct appropriate flatfields and co-add the data, this nonlinear, background transient response must be removed from the data. We found the most productive approach to be to treat the transient as a baseline to be subtracted from the data, A cubic curve is fitted to the time response for each pixel, allowing a floating window to mask out the step in flux attributable to a real source. Since each fully-sampled sky position was observed in four different pixels, we are able to iteratively adjust the floating window to encompass the correct time ranges for the pixels contributing to a source detection.

Standard image processing techniques are used to produce mosaic images. The library dark current is subtracted from the baseline background model and used to calculate a flat field response

for each pixel. The frames are aligned and coadded, weighted by the quality of the transient fit. Pixels with glitches and slew frames are excluded. Sources are identified in both space and time domains by examining both the mosaic and time history of each pixel; the sources reported in this paper are all strong, unambiguous detections. Photometric errors are estimated from the transient curve fitting statistics, the weighted data averages, and the observed RMS variation in the background of the mosaic; all error estimates agree to better than 10%.

Photometric measures for each identified source are computed from the sum of each contiguous pixel detected at the 3 sigma level or better. A factor of  $3.192 \text{ ADU } mJy^{-1} s^{-1} gain^{-1}$  (from the 1996 July calibration files, version 0711) was used to convert from detector units to flux units, and the fluxes were further scaled up by an empirical factor of 1.7 to account for the fact that faint sources will not reach their final stabilized responses in such short integrations. Due to uncertainties in properly calibrating non-stabilized data and possible systematic effects induced in the transient processing we estimate an additional overall uncertainty in the stated fluxes of about 30%. Faint ISOCAM source calibration is an ongoing area of investigation so these fluxes should be considered preliminary indicators of the true  $12\mu m$  flux. Positions were derived from flux-weighted averages for each contributing pixel and should be accurate to about  $\sim 12 \text{ arcsec}$ , an error that is dominated by the uncertainty introduced by jitter in the lens wheel position.

A sample CAM image of the source F14491+6040 is shown in Figure 2(a). The obvious source is a 17 sigma detection, with 84% of the flux in the brightest pixel.

## 2.2. ISOPHOT Observations

The ISOPHOT observations consist of chopped measurements with the C100 detector using the PHT22 Astronomical Observing Template (AOT), which provides 9 square pixels of size 43 arcseconds. The C90 filter with  $\lambda_c = 95\mu m$  and filter width  $51.4\mu m$  was used. For the initial measurements including the 9 sources we discuss here, a 32s on-source integration time was used. This was later changed to 64s for subsequent observations.

197 observations have been reduced using the default processing settings in version 6.1 of the ISOPHOT Interactive Analysis system (PIA, Gabriel *et al.* 1997) In addition the 9 sources discussed here were reduced carefully by hand using the PIA; these hand-reduced data used the ramp-subdivision option (with 9 or 16 readouts per ramp) to enable better de-glitching since this observing mode produces relatively few ramps per chopper plateau. In a few cases, the deglitching parameters were made slightly more stringent and some particularly noisy data were flagged out by hand. In all cases, the responsivities obtained from reduction of the Fine Calibration Source (FCS1) measurement within the AOT were used. In order to account for the size of the PHOT point-spread-function, which is larger than a single pixel, the ISOPHT central pixel (pixel 5) fluxes were **renormalized** by dividing by the intensity fraction of a centered point source falling on a single C100 pixel (0.61 at 90 urn; ISOPHOT Observers Manual p.14). The fields with ISOCAM detections were further **renormalized** to account for flux lost due to the observed offsets of the source away from the pixel center using a simple Gaussian beam model; these corrections range from a factor of 1.06 to 1.54.

The calibration uncertainty for chopped ISOPHOT measurements is not yet well understood, For example the ISOPHOT calibration is tied to staring measurements, whereas our chopped measurements are not fully stabilized and no transient response correction has been attempted. It is therefore only the instantaneous response of the detector which is measured, and it is likely this leads to underestimation of the source flux. For our particular observing mode and conditions (relatively low source brightness relative to the background) we estimate that the uncertainty is approximately **30%** in most cases.

Using this default reduction, the mean  $5\sigma$  sensitivity, **based on** the noise in the signal from pixel 5, is 71 mJy but varies strongly due to many factors including how long after the last detector curing the data were taken, what the cosmic ray hit rate was and possibly the flux history of the detector. Also, C100 occasionally enters a mode in which the response oscillates with a period comparable to the chopper plateau lengths obtained with the PHT22 AOT. The range of sensitivity for the observations reduced systematically is 16 to 421 mJy, again based on the central pixel. If

all the pixels except the four corner ones are summed, without flat fielding or chopper vignetting correction, the mean sensitivity becomes 102 mJy, with the range from 40 to 361 mJy.

### 2.3. Source Identification Procedures

A three way positional identification procedure was undertaken between the IRAS  $60\mu\text{m}$  position, the ISOCAM  $12\mu\text{m}$  position and candidate optical matches using IPAC's OPTID service (Lonsdale *et al.* 1997), taking into account the intrinsic positional uncertainties at each wavelength. These were taken to be  $15''$  at  $12\mu\text{m}$  and  $1''$  for the optical data (1a), which is derived, for the northern sky, from POSS I plates digitized by the Automatic Plate Measuring Engine in Cambridge (Irwin *et al.* 1994). For IRAS, the major and minor  $1\sigma$  positional uncertainties listed in the Faint Source Survey Database for each source were used. Full details of these identification procedures will be given in future papers (Hurt *et al.* 1998, Lonsdale *et al.* 1998 b); a brief description is given here.

The combined IRAS-ISOCAM positional uncertainties (typically  $17 \times 24$  arcseconds,  $1\sigma$ ) are large enough that the chance of false matches is significant. Therefore we first did a two-way IRAS-ISOCAM positional match, employing a careful analysis of the probability distribution of the matches, following the reliability techniques developed by Lonsdale *et al.* (1997)<sup>10</sup>. We then performed a simple two-way ISOCAM-optical match procedure based on positional coincidence alone, since the optical positional uncertainties are only of order 1 arcsecond, to select the optical candidate match for observing at the telescope. The third leg of the three way match procedure was then completed by checking the probability that the selected optical object is the correct match to the IRAS source, using the OPTID service. In 6 of the 8 detected sources the optical match was indeed confirmed by OPTID as the best optical match to the IRAS source. The exceptions

---

<sup>10</sup>A complicating factor in this procedure is that the background galaxy number counts at  $12\mu\text{m}$  must be known for this analysis, and these are as yet poorly defined, thus our identification procedures will refine with time as these counts become better measured.

are F15390+6038 and F16357+7658, for which the best optical match to the CAM source was misclassified by the APM plate measuring engine (used by OPTID) as a star rather than a galaxy. When optical source classifications are ignored for these two sources, the CAM-optical match for F15390+6038 is then found to indeed be the best optical match to the IRAS source. For F16357+7658, however, the optical galaxy at 16h33m51.6s+76d52m39s remains the best match to the IRAS source while a fainter galaxy at 16h33m51.8s+76d52m46s is the closest match to the ISOCAM detection. However, these two galaxies are an interacting pair, separated by 7". Since this separation is small compared to the IRAS-ISOCAM combined positional uncertainty for this source (16" x 18") it is likely that the 60 $\mu$ m and 12 $\mu$ m emission is associated with both galaxies of the pair, and integrated properties are therefore presented.

Details of the positional data are given in Table 1, which presents the IRAS-FSS position, the ISOCAM position, and the APM optical position, as well as the ISO-FSS, ISO-Optical and FSS-Optical positional offsets. The FSS-Optical offset is tabulated in units of the combined FSS-Optical uncertainty, dominated, of course, by the uncertainty in the infrared position. Note that the ISOCAM-FSS separations are all smaller than the typical  $1\sigma$  uncertainty of 17" x 24". There is evidence for a small systematic offset between the ISOCAM and the optical positions of 2" to 3" in declination.

We searched the literature and on-line databases for positional matches of our sources with any other known source at any other wavelength. Only F15390+6038, the high-excitation Sy2 galaxy in our sample, has any match within an arcminute, in this case in the NVSS radio database (Condon *et al.* 1997): NVSS J153956+602919, with 20cm flux density,  $S_{1.49GHz} = 3.6 \pm 0.4 mJy$ , lies 6.7" from the ISOCAM position (see Figure 1). The implied radio-infrared parameter,  $q = 1.82$ ,<sup>11</sup> for F15390+6038 is within the observed range for LIGs but 0.5 dex below the mean value,  $\langle q \rangle = 2.34$  (Condon, Anderson & Helou 1991), providing further evidence that this is a very active system. Although the fields of the other IIFGS sources are covered by the available NVSS survey database,

---

<sup>11</sup> $q$  is the dimensionless logarithmic far-infrared — 60 $\mu$ m plus 100 $\mu$ m — to 1.49GHz radio ratio (Condon, Anderson & Helou 1991)

none of the other sources is detected; this result is not surprising since IIFGS sources with normal  $q$  values are at the limit of the NVSS.

#### 2.4. Optical Imaging and Spectrophotometry

Ground based imaging and spectrophotometry are being obtained for IIFGS galaxies at Lick and Palomar Observatories in order to obtain redshifts, morphology, and optical/near-infrared photometry. The sources presented here were observed in 1996 June with the Lick Observatory 3-m Shane Telescope using the Kast Imaging Spectrograph under photometric conditions with fair (1.5") seeing. Spectra covering the wavelength region AA3500-10000 at  $5\text{\AA}$  resolution were obtained for redshift determination and imaging was obtained through "G" ( $\lambda_c \approx 4700\text{\AA}$ ;  $\Delta\lambda \approx 1215\text{\AA}$ ) and "I" ( $\lambda_c \approx 8275\text{\AA}$ ;  $\Delta\lambda \approx 1175\text{\AA}$ ) filters. The spectra were reduced with standard techniques using the IRAF reduction package. Virtually all of the galaxies showed strong emission lines characteristic of infrared galaxies. Redshifts are presented in Table 2, along with a list of the emission lines detected and a simple characterization of the excitation as AGN/Sy, Liner or HII following the technique originated by Baldwin, Phillips and Terlevich (BPT; Baldwin, Phillips & Terlevich 1981). Although, in principle, both the  $[\text{NII}]/\text{zcr}$  and  $[\text{OIII}]/H\beta$  ratios are necessary, in some cases the  $[\text{NII}]/H\alpha$  ratio is, by itself, sufficiently extreme to establish the excitation. The optical spectroscopic measures are comparable to nearby samples of LIGs, with values near the HII/Liner/AGN boundaries in the BPT excitation diagram (Smith, Lonsdale & Lonsdale 1998). There is one clear Seyfert 2 galaxy, F15390+6038, which exhibits very high excitation and emission-line velocity widths,  $\Delta v \approx 500 \text{ km s}^{-1}$ . The median  $H\alpha$  equivalent width,  $W_\lambda^{rest} \approx 40\text{\AA}$  is comparable to that for nearby LIGs (Veilleux *et al.* 1995) and significantly larger than typical equivalent widths of nearby (non-starburst) field galaxies (Kennicutt 1992).

Optical photometry was obtained from G( $\lambda 4700$ ) and I( $\lambda 8275$ ) band images obtained simultaneously through the Kast Spectrograph (0.78" pixels, approximately 2' FOV). Typically five 100s images were obtained in each filter, dithering the telescope by 5" -10" between images. Flat fields were obtained from median sky frames. The photometry was calibrated from filter transmission

data kindly measured for us by Rem Stone at Lick Observatory, convolved with our spectrophotometry of the standard stars BD+28 4211 and BD+33 2642. Photometry was done using the IRAF APPHOT package with 7" apertures. Statistical error in the photometry is typically 1-5%, much smaller than our estimate of systematic error of approximately 10–30% ( $1\sigma$ ). G and I flux densities are given in Table 3 and plotted in Figure 4. As a sample of the data, the central section of our mosaic images of F14491+6040 is shown in Figure 2 and the spectrum of this interacting pair is shown in Figure 3(a & b). Also shown in Figure 3(c) is the spectrum of F15390+6038, the highest excitation Sy2 system in this sample.

### 3. Results

The overall detection rates for the IIFGS sources are quite high:  $\sim 80\%$  at  $11.5\mu\text{m}$  for 418 fields processed as of 1997 October, and  $\sim 50\%$  at  $90\mu\text{m}$  for  $\sim 140$  sources at the  $5\sigma$  confidence level. These are fairly conservative estimates which are expected to improve as knowledge of the ISO instruments and data processing techniques improve.

For the 9 sources presented here the PHOT detection rate of 100% is not representative because we selected sources to observe spectroscopically based on detection by PHOT. One source is not detected by CAM, and for this same source, F13279+7840, no redshift could be obtained from the spectrum. For one additional source, CAM data have been obtained by the satellite but have not yet been delivered. We observed this source at Lick on the basis of the PHOT detection, since it has a very unambiguous optical identification. The remaining seven sources are all identified with strong emission line galaxies. The fact that the emission lines are so strong is additional support for the validity of the optical identifications with the infrared sources, since the likelihood of false association of the infrared sources with such strong emission line galaxies is very small.

The detailed optical to far-infrared photometric information for these 9 sources is given in Table 3, along with derived colors and mid- to far-infrared luminosities ( $H_0 = 75\text{km s}^{-1}\text{Mpc}^{-1}$ ,  $\Omega = 1$ ).  $60\mu\text{m}$  fluxes are given from the IRAS Faint Source Survey; these sources represent some of

the strongest 60 $\mu$ m sources in our sample. Also presented are coadded IRAS scan data from IPAC's SCANPI 1D coadders at both 60 and 100 $\mu$ m. As described above the ISO photometric calibrations remain somewhat uncertain; with an estimated uncertainty of order 30% for the *relative* calibration and perhaps as high as a factor of two for *absolute* flux densities for ISOCAM, with comparable values for ISOPHOT.

The spectral energy distributions for the 9 sources are plotted in Figure 4. The spectra are shown with an arbitrary offset, and the mid-infrared SEDs generally grow flatter from bottom to top of the plot. In two cases, IPAC's IRAS scan coaddition processor, SCANPI, has provided us with additional IRAS data:  $S_{12} = 0.05 \pm 0.03$  for F15390+6038 and  $S_{25} = 0.12 \pm 0.03$  for F13511+8238, where the uncertainties include systematic effects due to cirrus noise as well as the photometric uncertainties. These data points are included in Figure 4. In each case we have overplotted the IIFGS galaxy SED with the best match or matches from visual inspection of several characteristic nearby LIGs from Sanders *et al.* 1988. Three galaxies have SEDs which adequately fit most of the IIFGS data: Arp 220, an advanced merger and very dusty, compact nuclear starburst (eg. Smith *et al.* 1998, Sturm *et al.* 1996), UGC 5101 a high excitation Seyfert galaxy with AGN radio core (Lonsdale *et al.* 1998c), and Mrk 231, a warm source with a strong Seyfert 1 active nucleus and a QSO-class bolometric luminosity. An exception is F15390+6038 which is not well matched by any of the local LIGs; in this case we plot all three SEDs for comparison. Three galaxies are well matched by the SED of Arp 220. Four sources are reasonably well represented by the SED of UGC 5101, although two of these, F12513+7605 and F14403+6254 have a somewhat higher optical/mid-infrared flux-density ratio; in these cases the spectrum of Mrk 231 is also shown for comparison. F13511+8238 is well matched by Mrk 231. F15390+6038 has an unusual spectral-energy distribution showing an exceptionally large mid- to FIR flux-density ratio, but with a steep mid-IR to optical slope. One is tempted to use these SED relationships to draw inferences about the underlying energy sources for the IIFGS galaxies, but comparison of the energy distributions with luminosities or optical spectral excitation does not show any clear relationship between AGN excitation or bolometric luminosity and IR-to-optical SED, similar to the case for the nearby LIG sample (Smith, Lonsdale & Lonsdale 1998).

The observed redshifts agree well with the crudely predicted redshifts derived from the  $L_{60}$  vs.  $L_{60\mu m}/L_{blue}$  relation for three sources. For the rest of the sources the predicted redshifts are too high; this is due to the fact that the B band magnitudes measured from the archival Schmidt plate material by the APM measuring engine (as reported by OPTID) are systematically faint compared to the new G-band photometry by 0.2-1.5 mag, with the discrepancy increasing at fainter magnitudes. When the new photometry is used, all the objects lie on the same  $L_{60}$  vs.  $L_{60\mu m}/L_{blue}$  relation as the BGS sample (Figure 5a).

Two of the sources are identified with a clearly interacting galaxy pair: F14491+6040 and F16357+7658, and a further three show weak signs of tidal distortion: F12513+7605, F14541+6435 and F15390+6038. We have not attempted any image profile fitting or morphological classification, however it is likely that two of the sample, F14541+6435 and F14403+6254, are disk systems. F14491+6040 is a particularly interesting source, showing a pair of galaxies that are clearly interacting, with a tidal tail (Figure 2(b)). As shown in Figure 3, one of the pair shows HII excitation, and the other displays AGN excitation.

In Figure 5 we show the infrared/optical photometric relationships compared to a local LIG sample, the BGS (Soifer *et al.* 1987), and 24 infrared-selected QSOS (Cutri *et al.* 1998). Figure 5(a) shows that our selection for high far-infrared luminosity was successful since the 9 IIFGS galaxies inhabit the upper end of the  $L_{60}$  vs.  $L_{60}/L_b$  relation for LIGs. Indeed, two of our objects lie right at the tip of the distribution (although note that we have not included samples of “hyperluminous” infrared galaxies (Cutri *et al.* 1994) on this plot). The IR QSOS separate well from the LIGs in this diagram, and the IIFGS galaxies resemble the LIGs more closely. However in Figure 5(b) it is seen that two of the IIFGS galaxies are unusually high in  $L_{12}$  compared to the BGS sample, and one falls close to the region occupied by the IR QSOS. This object, F15390+6038 has the warmest mid-infrared SED of the sample, and also displays the strongest evidence for AGN excitation. It peaks strongly in the mid-infrared, falling steeply into the optical, showing an unusually large value of  $L_{12}/L_b$ . Thus it may be a new dust obscured QSO. F13511+8238 also has a  $12\mu m$  luminosity which is comparable to that of IR QSOS. It does not have a remarkably warm  $S_{60}/S_{12}$  color,

but it is the only object in our sample detected by IRAS at  $25\mu\text{m}$  ( $120\pm 30\text{mJy}$ ), with a very warm  $S_{60}/S_{25}$  color. Thus it too may be a new dust obscured QSO, though our spectroscopy has not identified any clear evidence for an active nucleus. Deep near-infrared spectroscopy of strong hydrogen lines or spectroscopy in polarized light of these two objects might reveal evidence for a dust obscured or scattered broad line region.

Two of the other objects which exhibit some evidence for AGN excitation, F13279+7840 and F16357+7658, show remarkably cool  $S_{60}/S_{12}$  colors, apparently cooler than any of the BGS galaxies (Figure 5(c); F13279+7840 does not appear in Figure 5(b) as it has no measured redshift). We note, however, that the k-correction for F16357+7658 is substantial (see Figure 4) and that there are several possible biases that could cause a tendency toward large  $S_{60}/S_{12}$  ratios in this sample. The first possible bias is due to the fact we can place a more sensitive limit on the  $S_{60}/S_{12}$  color than possible for most IRAS samples, including the BGS, because the relative sensitivity of the IRAS  $60\mu\text{m}$  band is so much higher than the IRAS  $12\mu\text{m}$  band. Indeed, not all of the BGS sample were detected by IRAS, even when the data were coadded using the SCANPI processor, as shown by the upper limits in Figure 5(c). Secondly, there may be a systematic tendency for the IRAS  $60\mu\text{m}$  fluxes of our sources to be overestimated, because they are close to the  $60\mu\text{m}$  sensitivity limit of the FSS: for sources just below the limit of a flux-limited sample, positive noise excursions bring a source into the sample while negative ones do not, so the average flux of sources near the threshold is boosted. Finally, we reiterate that the CAM photometry is still subject to some calibration uncertainty. We will address the influence of such biases in follow-up publications (Hurt *et al.* 1998, Lonsdale *et al.* 1998b) when the statistics of a large IIFGS sample are available and the calibration is more certain.

Figures 4 and 5(d) suggest that the longer wavelength photometry has a disappointingly high dispersion, but perhaps this was to be expected. The ISOPHOT  $90\mu\text{m}$  and those IRAS  $100\mu\text{m}$  fluxes which are available do not generally agree very well with one another, and there is a systematic offset between them with the IRAS  $100\mu\text{m}$  fluxes being higher than the ISOPHOT  $90\mu\text{m}$  fluxes. However, both the PHOT data and the IRAS  $100\mu\text{m}$  data have relatively low signal-to-noise,

and the ever-present concern about galactic cirrus-contamination of the photometry lends further uncertainty to the point source fluxes. Moreover, systematic sensitivity and calibration effects are still being assessed for the PHOT C100 AOT. Therefore we will leave a more detailed discussion of all our PHOT data to a later paper in this series; however we note that comparison to the BGS sample in Figure 5(d) does tend to support the PHOT fluxes as more reliable than the Scanpi  $100\mu m$  ones.

#### 4. Summary & Future Prospects

These first results from the ISO-IRAS Faint Galaxy Survey have shown that, if this small sample of 9 sources is representative of the whole, the IIFGS will be one of the largest and deepest samples of faint infrared-luminous galaxies available until the advent of WIRE (the Wide Field Infrared Explorer, Hacking *et al.* 1996) and SIRTf. The redshift range for this sample is  $0.1 \lesssim z \lesssim 0.4$ ; reasonably well predicted by use of the  $L_{60}$  vs.  $L_{60\mu m}/L_{blue}$  relation for those objects for which the APM-measured blue magnitudes turned out to be close to the new G band photometry. The ISOCAM detection rate is also impressively high - 80% for the sample of 418 IIFGS objects already processed - demonstrating that the IRAS galaxy selection techniques are highly robust against artefacts and cirrus-related sources. We can therefore expect that by the end of the ISO mission we will have on the order of 600 IIFGS galaxies with  $0.1 \lesssim z \lesssim 1.0$ , and  $10^{10.5} \lesssim L_{60} \lesssim 10^{13}$ ; an excellent sample for study of the evolutionary history of infrared-luminous galaxies up to  $\sim 5$  Gyr ago.

Our survey will also result in a serendipitous measurement of the  $12\mu m$  galaxy number counts, since our field of view is quite large. We have already accumulated over 1.25 square degree of deep CAM imaging to an  $11.5\mu m$  point source completeness limit of  $\sim 1.0$  mJy (corresponding to an  $\sim 10\sigma$  detection sensitivity), comparable to other dedicated ISO deep cosmological surveys. Our first measurement of the number counts will be presented by Lonsdale *et al.* 1998b.

The characteristics of the 9 sources we discuss here are similar to those of the much more local IRAS Bright Galaxy Sample. They span a similar range of  $60\mu m$  to  $12\mu m$  infrared spectral slope

and infrared luminosity. There is also evidence that the flatter spectrum sources are more likely to house an active nucleus, and our highest redshift source, F15390+6038, has the flattest infrared spectral energy distribution and displays a Seyfert 2 type optical spectrum. It seems very similar to several of the luminous infrared-selected QSOS (Cutri *et al.* 1998).

We wish to thank the staff of Lick Observatory for supporting the optical observations reported here, especially Rem Stone for measuring the filter curves. The ISOCAM data presented in this paper were reduced using a **deglitching** component of “CIA,” a joint development by the ESA Astrophysics Division and the ISOCAM Consortium led by the ISOCAM PI, C. Cesarsky, Direction des Sciences de la Matière, C. E. A.-Saclay, France. The ISOPHOT data presented in this paper was reduced using PIA which is a joint development by the ESA Astrophysics Division and the ISOPHOT consortium. This project has benefitted from the use of NED — the NASA Extragalactic Database — supported at IPAC by NASA and the STSCI Digitized Sky Survey images of the Palomar Observatory Sky Survey (POSS I). HES thanks IPAC for providing continuing support as a home away from home. IPAC/JPL is supported by NASA. Additional support of this project has been provided by NASA 1S0 grants to IPAC and to UCSD.

REFERENCES

- Baldwin, J. A., Phillips, M. M., & Terlevich, R. 1981, PASP, 93, 5
- Barvainis, R., Antonucci, R., Hurt, T., Coleman, P. & Reuter, H.-P. 1995, ApJ, 451, L9
- Cesarsky, C. *et al.* 1996, A&A, 315, L32
- Condon, J. J., Anderson, M., & Helou, G. 1991, ApJ, 376, 95
- Condon, J. J. *et al.* 1997, preprint.
- Cutri, R. M., Huchra, J. P., Low, F. J., Brown, R. L. and Vanden Bout, P. A. 1994, ApJ, 424, L65
- Cutri, R. M. 1998, pvt. communication
- Eisenhardt, P., Armus, L., Hogg, D. Soifer, B. T., Neugebauer, G., & Werner, M. 1996, ApJ, 461, 72
- Gabriel, C., Acosta-Pulido, J., Heinrichson, I., Morris, H. & Tai, M.-W. 1997, in *Astronomical Data Analysis Software & Systems VI*, A.S.P. Conf. Series, v. 125, eds. G. Hunt & H. Payne, (San Francisco: A. S.P.), p. 108
- Hacking, P. B. 1996, 388, 310
- Hurt, R. *et al.* 1998, in preparation
- Irwin, M. J. *et al.* 1994, *Gemini Newsletter No.* 37, Royal Astronomical Society. See also <http://www.ast.cam.ac.uk/lpinfo/apmcat/apmcat.html>
- Kennicutt, R. 1992, ApJ, 388, 310
- Kessler, M. *et al.* 1996, A&A, 315, L27
- Lemke, D. *et al.* 1996, A&A, 315, L64
- Lonsdale, C.J. *et al.* 1997, in IAU Symposium 179, *New Horizons from Multiwavelength Sky Surveys*, ed. B. McClean, (Kluwer:Dordrecht).

Lonsdale, C. J. *et al.* 1998a, in preparation

Lonsdale, C. J. *et al.* 1998b, in preparation

Lonsdale, C. J., Lonsdale, C. J., Smith, H. E., & Diamond, P. D. 1998c, in preparation

Moshir, M. M. 1995, ApJ, 123, 456

Sanders, D. B. *et al.* 1988, ApJ, 325, 74

Sanders, D. B. and Mirabel, F. 1996, ARA&A, 34, 749

Smith, H. E., Lonsdale, C. J., Diamond, P., Lonsdale, C. J. 1998, ApJ, in press

Smith, H. E., Lonsdale, C. J., & Lonsdale, C. J. 1998, ApJ, 492, in press

Sturm, E. *et al.* 1996 A&A, 315, 1,133

Soifer, B. T. *et al.* 1987 ApJ, 320, 238

VanBuren, D. *et al.* 1997

Veilleux, S. *et al.* 1995, ApJS, 98, 171

Fig. 1.— OPTID finding charts for the 9 sources in our sample. Each chart is 4' on a side. Symbols for ID type (star vs galaxy) are shown in the legend. optical candidates are numbered in order of the identification probability assuming the APM classification and magnitude. The IRAS ( $1\sigma$ ) error ellipse is shown by the solid elliptical contour and the CAM position is shown by the double circular contour, with radii 6" and 12". The position of the NVSS source in the field of F15390+6038 is indicated by the smaller double circle.

Fig. 2.— ISOCAM 11.5 $\mu$ m and optical imaging of F14491+6040. (a) The STScI Digitized Sky Survey image for this field. The region covered by the fully-sampled ISOCAM image is indicated by the dashed box, and the location of the ISOCAM source is indicated by the dashed circle. (b) The ISOCAM image is rotated to match the DSS Image; the entire fully-sampled image is shown, spanning 160" on a side. The field imaged at Lick is indicated by the dashed box. The Lick (c) G-band ( $\lambda 4700$ ) and (d) I-band ( $\lambda 8275$ ) images clearly show the double-nucleus counterpart to the ISOCAM detection as well as a probable tidal tail feature seen immediately to the north.

Fig. 3.— Lick red spectra of IIFGSLIGs. (a) F14491+6040a,  $z = 0.2779$ , is shown in Figure 2 to be interacting; this member of the pair shows HII excitation. (b) F14491+6040b,  $z = 0.2783$  (the redshift difference between "a" & "b" is not significant), shows AGN excitation. This spectrum has been lightly smoothed (3 pixel gaussian). (c) F15390+6038,  $z = 0.3769$  is the highest redshift galaxy in this sample of 9 and the clearest case of Sy2 excitation.

Fig. 4.— FIR – optical spectral energy distributions for the 9 IIFGS sources. Plotted are: 1) IRAS 100 $\mu$ m SCANPI flux density, 2) 90 $\mu$ m ISOPHOT flux density, 3) IRAS 60 $\mu$ m flux density (also 25 $\mu$ m and 12 $\mu$ m IRAS data where detected), 4) 11.5 $\mu$ m ISOCAM measure, and 5) Lick "I" ( $\lambda 8275$ ) and "G" ( $\lambda 4700$ ) band photometry. Spectra are ordered by steepness of the mid-infrared SED with arbitrary logarithmic offset. The IIFGS data points are connected by a dotted line. The SEDs of Arp 220 (pure starburst, solid line), UGC 5101 (intermediate AGN, long dashed line) and Mrk 231 (infrared QSO, short dashed line) are plotted for comparison. In each case we overplot the SED(s) which by visual inspection best match the IIFGS data. The spectrum of F15390+6038, a high-excitation Sy 2 galaxy, is exceptional, with warm infrared color, but steep IR-optical slope.

Fig. 5.— Distributions of flux-density ratios (colors) and luminosities for the 9 IIFGS galaxies compared to the local Universe Bright Galaxy Sample (BGS, Soifer *et al.* 1987) and infrared-selected QSOS (IRQSOs, Cutri *et al.* 1998). Panel (a) shows the F] R/Blue color —  $60\mu\text{m}$  luminosity relationship. (b)  $60\mu\text{m}/12\mu\text{m}$  color vs 12pm luminosity. (c)  $12\mu\text{m}/\text{Blue}$  color ratio vs 60pm/12pm color ratio. (d)  $60\text{pm}/100\text{pm}$  color ratio vs 60pm/12pm color ratio. The legend is the same for all panels, and is shown in panel (b) with additional symbols indicated in (d). No k-corrections have been applied to the data as plotted. Individual IIFGS galaxies are indicated by name in panels (b) and (c) when they fall off the general BGS relationships, **such as** the IRQSO-like F15390+6038. In panel (d) IIFGS galaxies are plotted twice if they have both an IRAS  $100\mu\text{m}$  detection and a PHOT  $90\mu\text{m}$  detection. Typical error bars for both ratios  $S_{60}/S_{90}$  and  $S_{60}/S_{100}$  are illustrated. Note that both the BGS and the IRQSOs include objects with only upper limits to the 12pm IRAS flux density.

TABLE 1  
SELECTED ISO-IRAS FAINT GALAXIES: POSITIONAL OFFSET DATA

IRAS Source	FSS POSITION		ISOCAM POSITION		OPTICAL POSITION		ISO-FSS		ISO-OPT		FSS-OPT
	$\alpha$	$\delta$	$a$	$\delta$	$a$	$\delta$	$\alpha$ (//)	$\delta$	$\alpha$ (//)	$\delta$	$\sigma^*$
F12513+7605	125254.4	+75 4929	125250.7	+75 4935	125252.43	+75 4935.5	13.7	-6.0	6.4	0.5	0.5
F13279+7840	132827.9	+78 2508			132826.88	+78 2522.4					0.5
F13511+8238	134946.1	+82 2343	134946.3	+82 2335	134948.94	+82 2328.4	-0.4	8.0	5.2	6.6	1.0
F14403+6254	144132.0	+62 4138	144130.5	+62 4138	144130.25	+62 4140.6	10.3	0.0	-1.7	2.6	1.2
F14491+6040	145021.8	+60 2825	145023.9	+60 2809	145023.51	+60 2811.5	-16.2	16.0	-3.6	2.5	1.7
F14541+6435	145506.7	+64 2342	145506.0	+64 2357	145505.44	+64 2403.0	4.5	-15.0	3.6	6.0	0.9
F15328+6133	153348.9	+61 2358	...		153347.48	+61 2358.7	.	.	.	.	1.5
F15390+6038	153958.8	+60 2911	153967.1	+60 2914	153957.21	+60 2915.4	12.6	3.0	0.8	1.4	1.1
F16357+7658	163352.4	+76 5234	163352.0	+76 5252	163351.77	+76 5245.8	6.4	-18.0	-0.8	-6.2	1.9

\* FSS-APM Optical positional offset in units of the combined FSS-Optical uncertainty.

TABLE 2  
SELECTED ISO-IRAS FAINT GALAXIES: SPECTROSCOPIC RESULTS

NAME	$z$	Detected lines	[NII]/H $\alpha$	[OIII]/H $\beta$	Excitation
F12513+7605	0.1676	H $\alpha$ , NII	0.26		HII/Liner
F13279+7840	...			...	
F13511+8238	0.2718	H $\alpha$ , [NII], [OIII]	-0.35	>0.5	HII
F14403+6254	0.1117	H $\alpha$ , [NII], [SII]	-0.13		HII
F14491+6040a	0.2779	H $\alpha$ , [NII], [SII], H $\beta$ , [OIII]	0.32	-0.18	HII
F14491+6040b	0.2783	H $\alpha$ , [NII], [SII], H $\beta$	-0.09	>0.5	AGN
F14541+6435	0.1995	H $\alpha$ , [NII], [SII]	-0.09		AGN/Liner
F15328+6133	0.3534	H $\alpha$ , [NII]	-0.40		HII
F15390+6038	0.3769	H $\alpha$ , NII, SII, H $\beta$ , [OIII]	-0.35	0.78	Sy2: $\Delta v \approx 500$ km/s (FWHM)
F16357+7658	0.2714	H $\alpha$ , [NII], [SII], [OIII]	0.00	>0.0	AGN/Liner

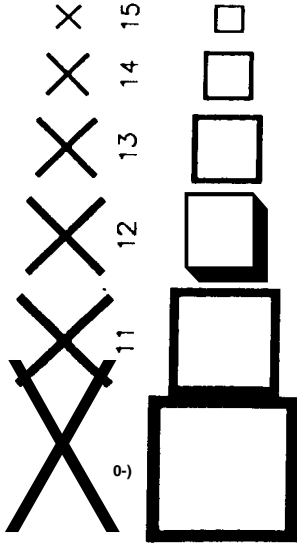
TABLE 3  
SELECTED ISO-IRAS FAINT GALAXIES: PHOTOMETRIC PROPERTIES

IRAS Source	60 $\mu$ m FSS (mJy)	11.5 $\mu$ m CAM (mJy)	90 $\mu$ m PHT (mJy)	60 $\mu$ m IRAS: SCANPI (mJy)	100 $\mu$ m SCANPI (mJy)	$B_{APM}$ (mag)	$\log_{10} S_{60}/S_B$	$S_{4700}$ (G) (mJy)	$S_{8275}$ (l) (mJy)	$z_{pr}$	$z_{obs}$	$L_{60}$ ( $\log L_{\odot}$ )	$L_{12}$	$\log_{10} S_{60}/S_G$
F12513+7605	159 $\pm$ 31	4.59 $\pm$ 0.16	166 $\pm$ 41	160 $\pm$ 20	320 $\pm$ 30	19.1	1.07	0.121 $\pm$ 0.006	0.37 $\pm$ 0.02	0.17	0.1676	11.12	1029	1.02
F13279+7840	161 $\pm$ 31	<0.6 (30)	164 $\pm$ 57	170 $\pm$ 20	<270 (3 $\sigma$ )	21.7	2.12	0.021*0.002	0.08 $\pm$ 0.01	0.83	.			1.80
F13511+8238	180 $\pm$ 32	1.78 $\pm$ 0.36	157*55	210 $\pm$ 20	400 $\pm$ 150	21.6	2.12	0.084 $\pm$ 0.004	0.17*0.01	0.80	0.2718	11.69	11.16	1.29
F14403+6254	163*30	4.51 $\pm$ 0.20	284 $\pm$ 71	220 $\pm$ 30	480 $\pm$ 50	19.8	1.36	0.150 $\pm$ 0.008	0.61 $\pm$ 0.03	0.26	0.1117	10.88	9.91	1.06
F14491+6040	135*25	2.08 $\pm$ 0.12	157 $\pm$ 32	140 $\pm$ 20	<540 (3 $\sigma$ )	19.8	1.28	0.100*0.005	0.35*0.02	0.25	0.2780	11.54	10.43	1.04
F14541+6435	155*31	2.88 $\pm$ 0.12	219*59	180 $\pm$ 20	4604c10	20.5	1.62	0.106*0.006	0.32 $\pm$ 0.02	0.40	0.1995	11.33	10.24	1.12
F15328+6133	282 $\pm$ 26		315 $\pm$ 76	340 $\pm$ 20	760 $\pm$ 50	21.0	2.08	0.036*0.004	0.16 $\pm$ 0.01	0.60	0.3534	12.15	.	1.87
F15390+6038	164 $\pm$ 28	20.36 $\pm$ 0.93	195 $\pm$ 55	200 $\pm$ 20	<300 (3 $\sigma$ )	20.4	1.64	0.020*0.002	0.06 $\pm$ 0.01	0.40	0.3769	11.99	1171	1.89
F16357+7658	271 $\pm$ 25	0.48 $\pm$ 0.08	272 $\pm$ 57	260 $\pm$ 20	39 O*100	19.6 (R)	2.30	0.044*0.004	0.09*0.01	0.85	0.2714	11.78	9.77	1.67

Chart scale = 3.37 "/mm

COSCAT:  $\circ$  = gal,  $\bullet$  or  $\bullet$  = s or  
 GSC/TIC:  $\square$  = gal,  $\times$  = star  
 FSDB (in center):  $\oplus$

COSCAT scale: Image size & shape  
 GSC/TIC magnitude scale:



[ ] = statistically corrected non-stellar mag.s.

